EGW 2014
3rd European Geothermal Workshop
Karlsruhe, 15-16 October 2014

Modelling location errors of the seismicity induced at Soultz-sous-Forêts

Xavier Kinnaert and Emmanuel Gaucher

KIT, Institute of Applied Geosciences, Div. of Geothermal Research, Adenauerring 20b, 76131 Karlsruhe, Germany

xavier.kinnaert@kit.edu

Keywords: Induced seismicity, location, uncertainties, local network

1. INTRODUCTION

Hypocentre location is one of the most important characteristic of any seismic event since many other seismic parameters can be derived from it (e.g. magnitude, focal mechanism) and several interpretation will also be based on it (e.g. geothermal reservoir extension). Thus knowledge of its reliability or, similarly, quantification of the location uncertainty is of importance prior to further use of this information and result interpretation.

The study presented here aims at modelling seismic event location uncertainties, in the case of the geothermal site of Soultz-sous-Forêts (Alsace, France). Many seismological analyses have already been done on this research site because the numerous hydraulic stimulations which were performed induced seismicity. We focus here on the seismicity induced during the deep stimulation of the GPK2 well, carried out in 2000. This stimulation was monitored by several seismic networks and the seismic data processing was done using different combinations of networks and different velocity models (Dyer 2001, Cuenot et al. 2008). Also, 4D tomography was conducted (Cuenot et al. 2008, Calò et al. 2011) as well as inversion of the stress-field changes over time and depth based on the event focal mechanisms (Schoenball et al. 2014). Therefore, our analysis is a first step to characterize the effect of seismic location uncertainties in further processing of this basic attribute.

In the following, we investigate the effects induced by the use of the different seismic monitoring networks. We also compare results obtained by two different location methods. Finally, we start looking at the effect generated by velocity model changes.

2. FIELD DESCRIPTION

2.1. GPK2 induced seismicity

In our modelling work, we focus on the stimulation of well GPK2 carried out in 2000. During this stimulation, 23400 m³ of water were injected over ~6 days, in the 4400 – 5000 m depth interval (Cuenot et al. 2008). The forced water injection induced several 10,000 seismic events with a maximum magnitude of Mw=2.5 (Dorbath et al. 2009). The seismicity is roughly oriented in a vertical plane striking in the N150°E direction (Figure 1). The extension of the main part of the cloud is about 1500 × 500 m² horizontally and covers the depth interval between 4000 and 5500 m. All the (visible) seismicity is located in the crystalline formation which starts at a depth of ~1400 m.

2.2. Seismic network at Soultz-sous-Forêts

To monitor the GPK2 stimulation, several seismic networks were installed (Figure 1). A downhole network (red triangles) was recording using 3 4-C accelerometers and 2 hydrophones from a depth close to the top of granite or within the granite (Cuenot et al. 2008). Unfortunately, 1 hydrophone (EPS1) came out of order early in the stimulation phase. This network alone detected ~31,500 seismic event candidates among which ~14,000 were located (Dyer 2001). On the surface, a temporary network composed of 8 1C-seismometers and 6 3C-seismometers was deployed over the field (green triangles). On this network, ~11,000 seismic events were detected and by combining the surface records with the associated downhole records, Cuenot et al. (2008) located ~7,000 events. Three permanent surface 3C-seismometers maintained by the ReNaSS were also recording but the associated seismograms were never used for locating the events. The epicentres shown in Figure 1 are those obtained by Calò et al. (2011) for the same set of 7,000 events, after 4D tomography.

3. METHODOLOGY

In the following, we assume that seismic event location is computed using the onset times of the P- and S-waves arrivals observed on the seismograms. Therefore, locating consists in finding a hypocentre and an origin time which best explain these arrival times within given velocity models (one for the P-wave and one for the S-wave). The modelling of location error of seismic events will consist of 2 main steps. In the first step, forward modelling is performed to generate synthetic arrival times at the network stations which will be used for the inverse problem during the second step. However, between the first and the second step, several hypotheses are made to perturb the original synthetic data. Hence, uncertainties in the P- and S-wave arrivals are attributed and we investigate location uncertainties as a function of the seismic network used, as a function of the inverse problem set-up, and as a function of velocity model changes. Besides the location uncertainties, the location accuracy will also be studied.

3.1. Forward modelling

3.1.1. Location of the synthetic seismic events

A synthetic cloud of regularly spaced seismic sources (every 250 m) covering the location of the seismicity induced in 2000 is defined. The dimension of the synthetic meshed zone is roughly 1.25 × 2.25 km² horizontally and 1.5 km in depth, covering the depth interval 4000 to 5500 m TVD (red crosses in Figure 1). For simplicity in the modelling, the geographical coordinate system is rotated around the vertical axis to become aligned with the main direction of the induced seismicity (N150°E). All results will be later shown in this coordinate system, with horizontal axes Xc and Yc (blue segments in Figure 1).

3.1.2. Velocity model

For the modelling of errors independent from the velocity model, we use the initial velocity model proposed by Cuenot (2009). Eight flat layers with constant velocities are considered but the Vp/Vs ratio is not constant. Vp varies between 1850 and 5800 m/s (at 1800 m TVD MSL) and Vs between 860 and 3310 m/s. So, at the depth of the induced seismicity, the velocity model is taken homogeneous. The surface stations of the network are all located in the first (slowest) layer of the model. The sensors installed in boreholes are sitting in the deepest layer (for both hydrophones) or in the 2nd layer before last.

3.1.2. Travel-times of seismic body waves

To calculate the propagation time, between the synthetic locations and the receivers of the different networks, for both P- and S-waves, the codes developed by Podvin and Lecomte (1991) are used. These routines are numerical solvers of the eikonal equation in isotropic heterogeneous acoustic media where wave kinematics is represented by a distribution of slowness. A finite differences scheme is used. A 15-m 3D mesh was used to sample the Soultz velocity model (or inversely slowness model).

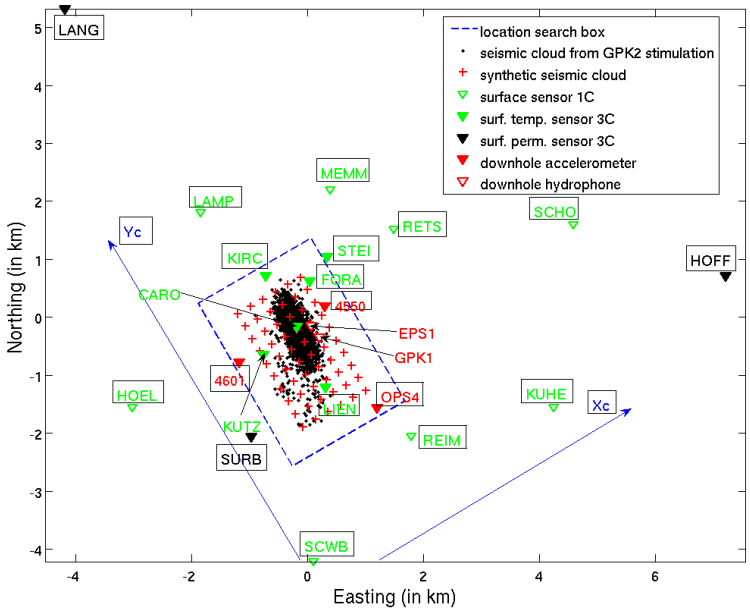

Figure 1: Map of Soultz-sous-Forêts during GPK2 stimulation showing the epicentres of the induced seismicity (black dots) and the seismic networks: the temporary and permanent surface networks (green and black triangles) and the downhole network (red triangles). Empty triangles represent mono-component sensors and filled triangles 3-components sensors. The geometry of the modelling is also displayed highlighting the simulated epicentres (red crosses) as well as the new coordinate system (axes Xc and Yc) and the projection of the location box for grid-search (see text for details).

3.2. Inverse problem

From a set of computed travel-times on a given network, the inverse problem consists in finding the associated location. However, prior to this step, uncertainties on these times were attributed to represent picking uncertainties as observed by previous studies. Accordingly, a 5 ms uncertainty was attributed to any arrival time observed on the downhole network, for both P- and S-waves (Dyer 2001), and a 15 ms uncertainty to both waves of the temporary surface network (Cuenot 2009).

As reference method to locate the events, a non-linear approach which works within any type of velocity model and provides complete spatial description of the probability density function of the locations is chosen. The NonLinLoc software from Lomax et al. (2000) is applied. To quantify the misfit between the observed (simulated) and the theoretical travel-times, the likelihood function is that described by Tarantola and Valette (1982) and is associated to a least-square fit of weighted residuals. In addition to the NonLinLoc software, the Hypoellipse software from Lahr (1999) is also applied. The latter uses a linear inversion approach. Then, we can discuss possible result differences between both codes.

The location result consists in a most probable location for each event as well as the associated uncertainties. With the linear inversion technique, the uncertainties are assumed Gaussian and the principal direction and length of the error ellipsoid for 1

standard deviation (or 68.3% probability that the event is located in this volume) are provided. Such a result may also be output from the non-linear inversion approach. However, the latter can provide a full geometry of the location probability density and can therefore better describe location complexity.

4. RESULTS

4.1. Location results as a function of the network

Dyer (2001) located the induced seismicity recorded by the downhole network only. On the contrary, Cuenot (2009) located the induced seismicity by adding the information obtained on the temporary surface network. Figure 2 shows the largest location uncertainties (at 1 standard deviation, or 68.3% cumulated probability) for the different network combinations and using the picking uncertainties mentioned by both authors, for horizontal sections at 4750 m depth (in the middle of the seismic cloud). As shown, the combination of both networks provides the smallest location uncertainties, between 55 and 70 m, which is in accordance with Cuenot (2009) effective results.

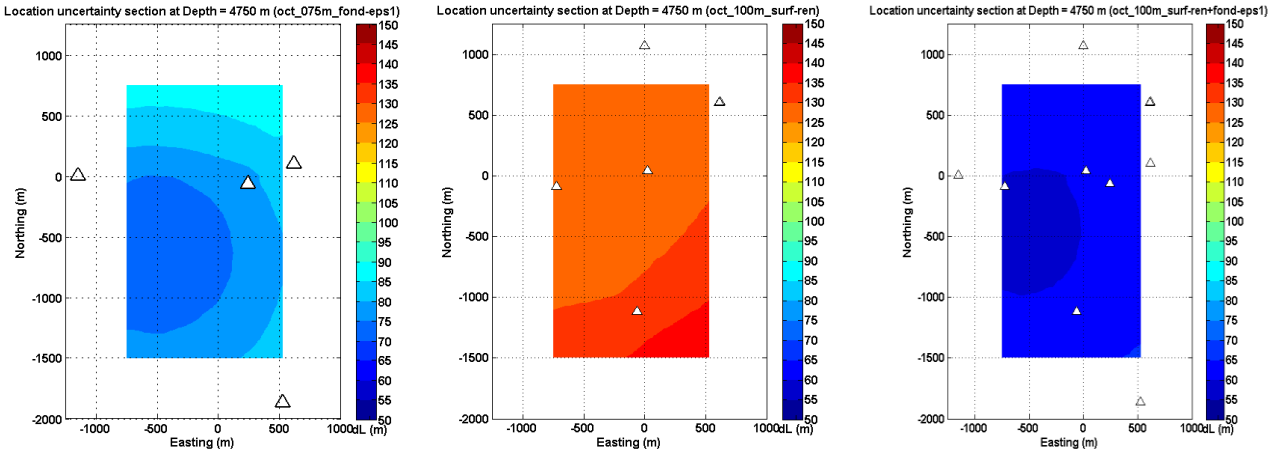

Figure 2: Horizontal sections at 4750 m depth of the largest location uncertainties modelled for the downhole network without EPS1 station (left), the temporary surface network (middle) and the combination of both (right). The seismic stations within the locating-box are displayed as white triangles.

The network coverage of the combined solution exhibits smaller uncertainties in the south-west part of the seismic cloud, very similar to the downhole network alone. Of course, with increasing depth, the uncertainties also increase and can reach 75 m at 5500 m MSL. So, an improvement of more than a factor 2 is obtained in the final location uncertainties by including the downhole network to the temporary surface network. In addition to the increased coverage of the network in the depth dimension, the more accurate pickings obtained, because of higher signal frequency content and quieter environment, play a role.

Obviously with this test, no location inaccuracies are observed (at the scale of the mesh cell) whatever the network used.

4.2. NonLinLoc vs. Hypoellipse locations

Here, we compare the location results of the NonLinLoc software and of the Hypoellipse software, which were obtained using the surface temporary network and the downhole network without EPS1 station. Figure 3 highlights on a depth projection the obtained results. At worst, the NonLinLoc hypocentres mismatch the theoretical locations by 9 m which is smaller than the grid cell (15 m). However, the Hypoellipse hypocentres exhibit larger inaccuracies. They are not due to the linearization of the location problem, but to the given accuracy of the P- and S-arrival times, which cannot be better than 0.01 s. So, these picking inaccuracies, which are introduced in the input data, induce location inaccuracies as high as ±40 m along East and North and between -100 m and 30 m in depth. Moreover, the depth inaccuracy tends to increase with the event theoretical depth; simultaneously the origin time tends to be earlier than theoretically. Although the provided picking accuracy may be smaller than the picking uncertainty (e.g. 15 ms for the surface network), the inversion problem does not provide similar result since it cannot take into account this initial inaccuracy. With regards to the location uncertainties, which still remain, Hypoellipse gives smaller uncertainties than NonLinLoc, along the main direction axis. The median of the differences is ~20 m with a maximum difference of 35 m. The directions of the main axes are comparable in both methods.

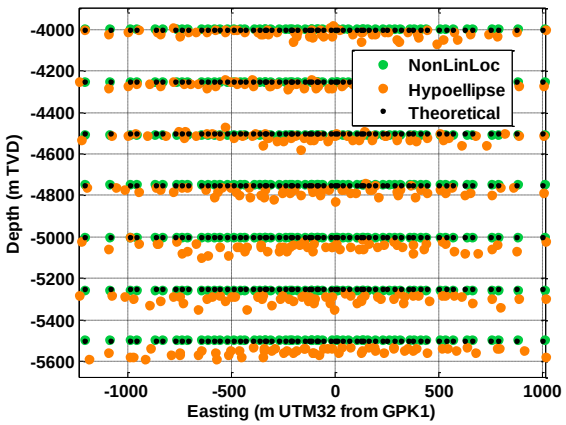

Figure 3: Depth projection of the events located using NonLinLoc (green points), Hypoellipse (orange points) and the expected depth location (black dot). The surface temporary network and the downhole network without EPS1 station were used to locate.

4.3. Location in an incorrect velocity model

Locating seismic events within incorrect velocity models should probably be considered as the usual case. At Soultz, this was considered in several tomographic studies (Charléty et al. 2006, Cuenot et al. 2008, Calò et al. 2011, Calò and Dorbath 2013). Our motivation here is to model and to discuss effects on event locations due to velocity model changes, both in terms of uncertainty and inaccuracy.

The first test consists in locating the synthetic events in the velocity model described earlier. However, the synthetic travel-times of the body-waves for the corresponding events have been computed in another velocity model. This model is similar to the other one except for one layer, between 4400 and 5000 m TVD, where the Vp and Vs velocities were decreased by 10%. This 600 m depth interval corresponds to the interval where the injection took place and where most of the seismicity occurred during GPK2 stimulation.

Contrarily to the previous tests, perturbation of the velocity model leads to location inaccuracies. With the 10% perturbation, inaccuracies up to 75 m may be obtained and apply to more than 30% of the synthetic events (Figure 4). They increase with depth once the event is located in or below the perturbed velocity layer. A similar effect is observed with the estimate of the occurrence time of the events which happens later than expected when the event is located in or below the perturbed layer. The inaccuracies in the epicentre locations are symmetrical around a point located in the SE quarter of the synthetic cloud and increase with the offset to this point. Hence, the distribution of inaccuracies is network design dependent. Depth inaccuracies are larger than horizontal ones.

Due to the picking uncertainties, location uncertainties apply to the "mis-located" events and range between 50 and 76 m in our tests. Hence, these uncertainties are of the order of the location inaccuracies.

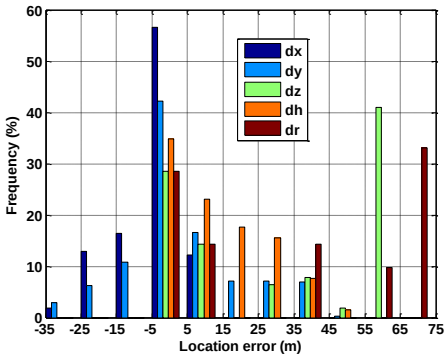

Figure 4: Location inaccuracies of the synthetic events located, in the wrong velocity model, using the downhole and the temporary surface networks.

Figure 5 shows the time residuals of all synthetic events as a function of depth for the downhole network without EPS1 station and for the temporary surface network. In both cases, the residuals are below the picking uncertainties assigned to the associated stations. The P-wave residuals have a range larger than the S-wave one. The residual range increases with depth once the synthetic event is located in or just below the perturbed layer. When the event is located deeper, the residuals tend to slightly decrease.

Downhole network

Temporary surface network

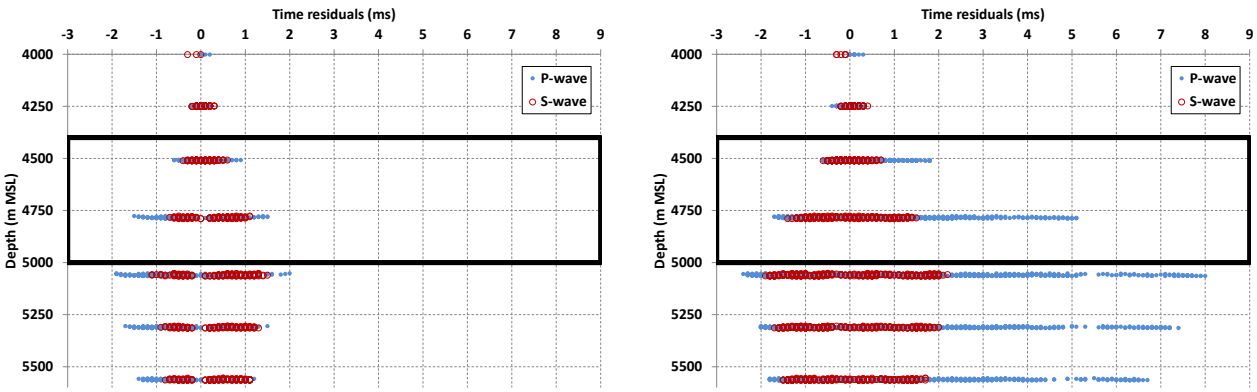

Figure 5: Time residuals of all synthetic events as a function of depth for the downhole network without EPS1 station (left) and for the temporary surface network (right). The events were located using both networks together. The black rectangle shows the depth interval were the P- and S-wave velocities has been decreased by 10%.

Usually, the residuals obtained at the stations are averaged and introduced as a station correction factor. By applying this approach, the origin time of the seismic events changed to become almost equivalent to the expected one, but the locations remained the same. The final residuals decreased in average but, of course, increased for the events located above the perturbed layer.

5. CONCLUSIONS & PERSPECTIVES

At Soultz, the use of the downhole network information decreases the location uncertainties by more than a factor 2 (compared to the temporary surface network alone), leading to 50 to 75 m uncertainties under usual processing conditions. Uncertainties are not distributed homogeneously within the seismic cloud and do not follow the seismic cloud shape. They are rather symmetric around a point located in the SW quarter of the cloud and increase with depth. These uncertainties appear to be of the same order as location inaccuracies when the velocity model is perturbed by 10% over the stimulation depth interval. In addition to these location inaccuracies, uncertainties from 50 to 75 m are also observed which means that both effects may be cumulated. The truncation or

Even in a perfectly know velocity model, truncation or rounding of observed arrival times can lead to systematic location bias in depth and origin time, as a function of depth. Location uncertainty will still be added to this inaccuracy.

So far, the location inversions were based on single or independent event approaches. It is planned to continue this analysis with multiple event approaches such as HypoDD location software, based on the double-difference principle. Moreover, we expect to investigate location inaccuracies and uncertainties within a velocity model which would be representative of the structural geology of Soultz geothermal reservoir, which is located in a horst.

ACKNOWLEDGMENTS

We thank the GEIE "Heat Mining" and particularly N. Cuenot who gave us access to the reports of the downhole network data processing. M. Calò provided us the final locations of the seismic events induced during the 2000 stimulation of GPK2 obtained after the 4D tomography. This work is supported by the EnBW Energie Baden-Württemberg AG, the Strasbourg University and is made under the framework of the LABEX ANR-11-LABX-0050_G-EAU-THERMIE-PROFONDE. It is funded by EnBW and the French National Research Agency as part of the "Investments for the future" program.

REFERENCES

Calò, M. & Dorbath, C. 2013. Different behaviours of the seismic velocity field at Soultz-sous-Forêts revealed by 4-D seismic tomography: case study of GPK3 and GPK2 injection tests. *Geophysical Journal International* **194**, 1119-1137.

Calò, M., Dorbath, C., Cornet, F.H. & Cuenot, N. 2011. Large-scale aseismic motion identified through 4-D P-wave tomography. *Geophysical Journal International* **186**, 1295-1314.

Charléty, J., Cuenot, N., Dorbath, C. & Dorbath, L. 2006. Tomographic study of the seismic velocity at the Soultz-sous-Forêts EGS/HDR site. *Geothermics* **35**, 532-543.

Cuenot, N. 2009. Réponse du granite fracturé de Soultz-sous-Forêts à des injections massives de fluide : Analyse de la microsismicité induite et du régime de contraintes. Vol. Ph.D., pp. 318. University of Strasbourg.

Cuenot, N., Dorbath, C. & Dorbath, L. 2008. Analysis of the microseismicity induced by fluid injections at the EGS site of Soultz-sous-Forêts (Alsace, France): Implications for the characterization of the geothermal reservoir properties. *Pure and Applied Geophysics* **165**, 797-828.

Dorbath, L., Cuenot, N., Genter, A. & Frogneux, M. 2009. Seismic response of the fractured and faulted granite of Soultz-sous-Forêts (France) to 5 km deep massive water injections. *Geophysical Journal International* **177**, 653-675.

Dyer, B.C. 2001. Soultz GPK2 stimulation June/July 2000. In: *Semore Seismic Report* Seismic monitoring report, SOCOMINE.

Lahr, J., C. 1999. HYPOELLIPSE: A Computer Program for Determining Local Earthquake Hypocentral Parameters, Magnitude, and First-Motion Pattern. In: *Open File Report 99-23, Version 1.1* (ed. USGS), pp. 119.

Lomax, A., Virieux, J., Volant, P. & Berge-Thierry, C. 2000. Probabilistic Earthquake Location in 3D and Layered Models. In: *Advances in Seismic Event Location*, Vol. 18 (eds. C. Thurber & N. Rabinowitz), pp. 101-134. Springer Netherlands, ISBN 978-90-481-5498-2.

Podvin, P. & Lecomte, I. 1991. Finite difference computation of traveltimes in very contrasted velocity models: a massively parallel approach and its associated tools. *Geophysical Journal International* **105**, 271-284.

Schoenball, M., Dorbath, L., Gaucher, E., Wellmann, J.F. & Kohl, T. 2014. Change of stress regime during geothermal reservoir stimulation. *Geophysical Research Letters* **41**, 1163-1170.

Tarantola, A. & Valette, B. 1982. Inverse problems = quest for information. *Journal of Geophysics* **50**, 159-170.